Data Assimilation Applied to the Temperature and Circulation in the Tropical Atlantic, 1983–84

JAMES A. CARTON AND ERIC C. HACKERT

Center for Ocean-Land-Atmosphere Interactions, Department of Meteorology, University of Maryland, College Park, Maryland

(Manuscript received 21 April 1989, in final form 2 January 1990)

ABSTRACT

A hydrographic dataset based on data from the SEQUAL/FOCAL experiment is used to determine the errors of a numerical simulation of the complete temperature and velocity fields of the tropical Atlantic during the two-year period 1983–84. To improve the accuracy of the analysis we develop an application of four-dimensional data assimilation. In this analysis the thermal fields of the model are updated once a month using sea surface temperature measurements and observed temperature profiles.

Much of the paper describes comparisons between differing analyses using data assimilation and the numerical simulation, and verification of these with temperature and velocity data from moored instruments. Assimilation of the temperature observations improves the accuracy of the temperature analysis. The amplitude of seasonal changes in the meridional thermal gradient is doubled at 38°W, bringing the analysis closer to the observed thermal gradient. At 28°W the improvement is less dramatic. The zonal thermal gradient at the equator is increased, but the month-to-month variability also increases significantly.

Comparisons are made with temperature and velocity measurements at midbasin mooring sites. Here assimilation sharpens and lowers the thermocline and reduces long-term trends in the thermal field. Assimilation also improves some features of the velocity field such as the depth and eastward penetration of the undercurrent core and the strength of the North Equatorial Countercurrent.

1. Introduction

This paper presents an application of four-dimensional data assimilation by producing an analysis of the tropical Atlantic Ocean during the two-year period (1983–84) of the Seasonal Response of the Equatorial Atlantic/Français Océan et Climat dans l'Atlantique Equatorial (SEQUAL/FOCAL) Experiment. In the tropical Atlantic Ocean changes are dominated by the seasonal cycle. A northward shift of the intertropical convergence zone of the wind field in boreal spring causes a seasonal tilt of the thermocline along the equator (shown in Fig. 1), as well as development of zonally oriented ridges and troughs in the thermocline. Associated with these meridional shifts in the thermal field are accelerations of zonal currents—westward near and a few degrees south of the equator (South Equatorial Current), and eastward within a few degrees of 5°N (North Equatorial Countercurrent). The timing and intensity of these events vary from year to year, as happened in early 1984. Then, the relaxation of the unusually strong trade winds in late 1983 caused an anomalous leveling of the equatorial thermocline. This led to anomalously high surface temperatures in the Gulf of Guinea (see Philander 1986).

Corresponding author address: Dr. James A. Carton, Center for Ocean-Land-Atmosphere Interactions, Department of Meteorology, University of Maryland, College Park, MD 20742.

The SEQUAL/FOCAL experiment was designed around the realization that disturbances in the tropical oceans propagate rapidly from one side of the basin to the other so that understanding the forces driving the seasonal cycle at one location requires knowledge of seasonal changes elsewhere. Even though an extensive set of observations was collected (summarized in a SEQUAL/FOCAL issue of *Geophysical Research Letters*, August 1984) it was not possible to collect enough measurements of all variables throughout the basin. Therefore some assumptions would be needed to interpolate between the sparse, noisy observations to construct complete fields of velocity and temperature as a function of time.

A number of methods of assimilating observations have been proposed. These include inverse methods, Kalman filtering, and adjoint methods, which are discussed in Ghil (1989) and other papers in the special issue of *Dynamics of Atmospheres and Oceans* in May 1989. One of these approaches, four-dimensional data assimilation has the particular advantages of straightforward implementation, computational efficiency, and flexibility. However its recent application to ocean circulation (e.g., Robinson et al. 1986; Moore et al. 1987; Hayes et al. 1989; Derber and Rosati 1989) has raised concerns about the importance of noise induced by the updating procedure and the problem of sparse and irregular data coverage of the oceans, which are difficulties for all data assimilation methods.

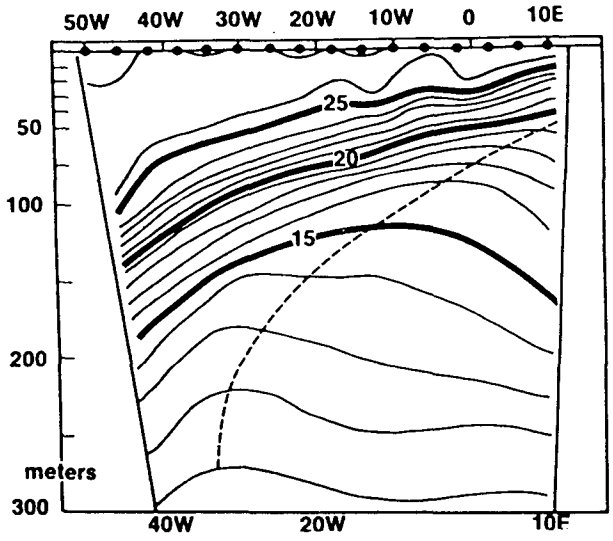

FIG. 1. Mean annual temperature in the 0°–2°S band with longitude and depth, reproduced from Merle (1980).

Our application of four-dimensional data assimilation uses the multilevel primitive equation model of Philander and Pacanowski (1986), to provide a first guess of the temperature and velocity fields throughout the tropical Atlantic basin. The temperature field of each model level in the upper 484 m is updated monthly using observations of temperature (surface temperature and temperature profiles). A temperature profile dataset has been constructed especially for this purpose and includes over 8000 profiles. A companion paper, Carton and Hackert (1989) describes the updating method in detail. The focus of this paper is on verification of the analysis, which is carried out using temperature residuals, eight inverted echo sounder moorings, and two moorings instrumented with temperature and velocity recorders.

To determine the quality of our data assimilation analysis (A3) we construct three alternative analyses. The first is a numerical simulation using the Philander and Pacanowski model without any updating (A1). The second is similar to our data assimilation analysis, except that climatological monthly temperature is used to provide a first-guess field for the temperature analysis (A2). This approach is similar to that used in the earliest analyses of atmospheric circulation. In the third alternative analysis the four-dimensional data assimilation is modified to determine the sensitivity of the analysis to assumptions about the velocity field (A4). Sections 2 and 3 describe the dataset and the data assimilation procedure. In sections 4 through 7 we describe the four analyses and examine their accuracy by comparing them to the independent observations. The data assimilation procedure is shown to improve the accuracy of the analysis substantially compared to these independent observations.

2. Observations

A major source of hydrographic observations (20°S–20°N) for 1983–84 is research data collected as a part of the SEQUAL/FOCAL experiment. FOCAL conductivity-temperature-depth (CTD) and hydrographic station surveys were conducted mainly between 5°S–5°N (Hisard and Henin 1987). Together with expendable bathythermeograph (XBT) data to depths of 300–500 m, the SEQUAL/FOCAL data represents 40% of the total tropical Atlantic hydrographic dataset during 1983–84. High quality hydrographic data, obtained through the National Oceanographic Data Center, have contributed another 35%. The remaining 25% comes in the form of bathymessage reports carried over the GTS system, and included in the Master Oceanic Observation Data Set (MOODS; Teague et al. 1987).

Before using this dataset, it has been checked for duplicate reports and for errors in the recorded position and time of observations. Erroneous station location reports can be identified as observations which do not appear in sequence along identifiable ship- or plane-tracks. Because of errors in nearsurface XBT temperature estimates caused by the time required to equilibrate to the surrounding temperature, the ocean surface temperature estimate is taken to be the same as the 5 m depth estimate. The observations are grouped into 1° × 1° × 5 day bins and averaged. The monthly binned data distribution is shown in Fig. 2. The monthly sea surface temperature dataset has been provided by J. Servain (Servain et al. 1987) based on observations collected from merchant ships.

3. Data assimilation procedure

The four-dimensional data assimilation procedure begins with a first guess of the three-dimensional fields of temperature, salinity, and possibly velocity. These first-guess fields may be provided either by a climatological dataset or by a numerical simulation. The first-guess temperature fields are then corrected by a series of updating steps carried out on the fifteenth of each month of the analysis. The corrected fields become that month's *analysis* of the state of the ocean, and may also be used as initial conditions for a numerical integration providing the first-guess fields for the next month's analysis.

a. First-guess fields

The first-guess fields for the data assimilation analysis A3 and analysis A4 and for the simulation referred to as analysis A1 are provided by the primitive equation model of Philander and Pacanowski (1986). The model domain extends from 30°S to 50°N with 1° × ⅓° horizontal resolution in the tropics, expanding toward higher latitudes for greater computational efficiency. Vertical resolution is 10 m at near-surface, expanding to coarser resolution with depth, for a total

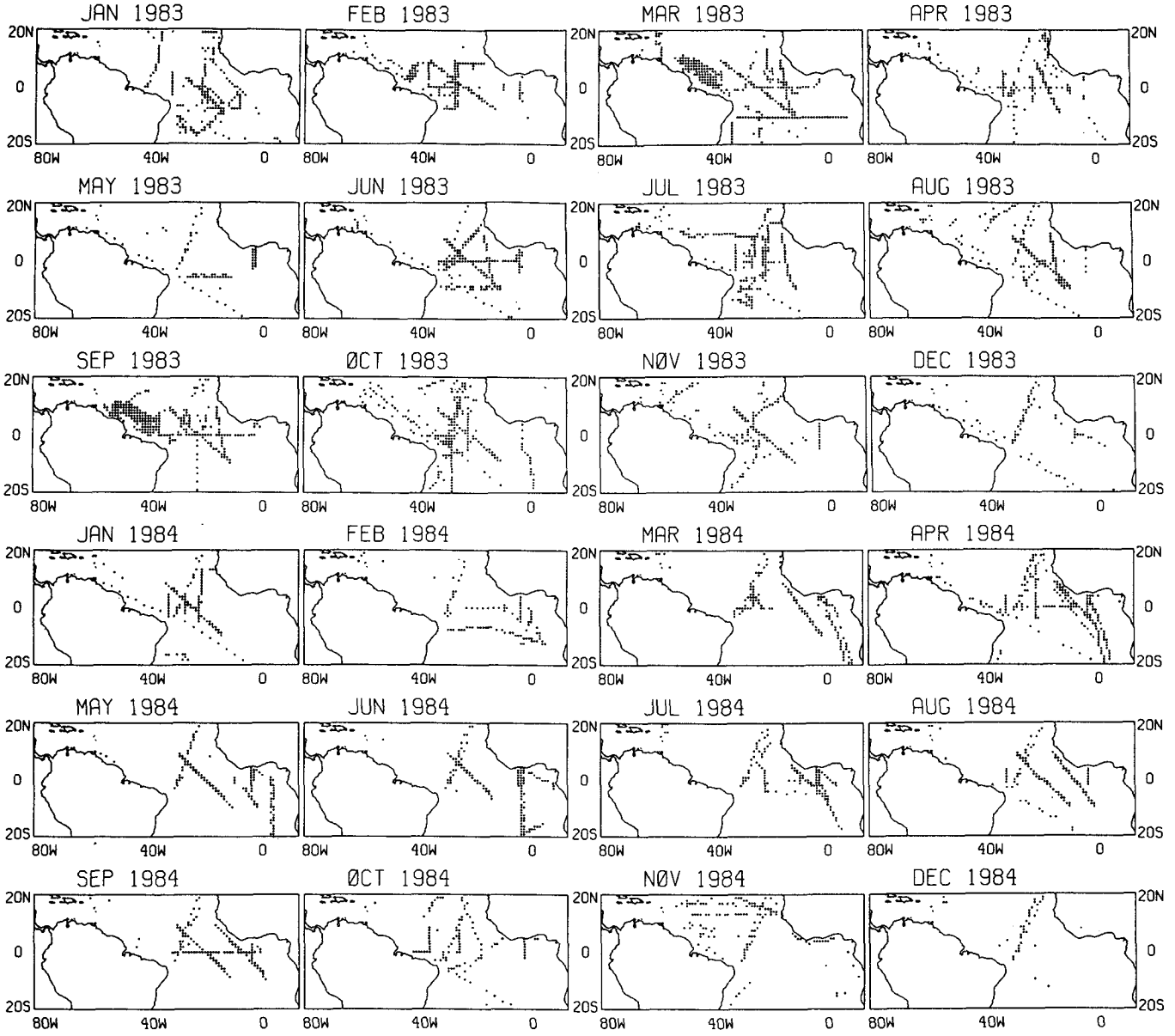

FIG. 2. Hydrographic data coverage month by month for 1983–84 between 20°S–20°N. Each dot represents at least one data point within a 1° × 1° bin. This data is used to provide updating for the analyses in Table 1.

of 27 vertical levels. Horizontal mixing of temperature and momentum is carried out with Laplacian diffusion using a diffusion coefficient of 2×10^7 cm^2 s^{-1}. Vertical mixing is Richardson number dependent, increasing with increasing vertical shear with the suggested formulation of Pacanowski and Philander (1981).

The model is forced at the surface with monthly surface winds provided by V. Cardonne (personal communication), based on the European Centre for Medium Range Weather Forecasts (ECMWF) wind product with the wind directions corrected to be consistent with ship wind observations. Surface heating due to incident solar radiation is assumed to have a constant value corresponding to its climatological average. Sensible and latent heating are estimated from a bulk formula which depends on the air–sea temperature contrast where climatological seasonal air temperature is specified (described in Philander and Pacanowski 1986). Initial conditions in 1983 are provided by Levitus (1982) climatological January temperature and salinity.

b. Mixed-layer temperature updating

The most extensive oceanic dataset available is of surface temperature. Indeed, we believe observed sur-

face temperature is a better estimate of the mixed layer temperature than the mixed layer temperature predicted by a model or climatology. We make use of this information by updating the model-predicted temperature in the following way. On the fifteenth of each month the model-predicted mixed layer depth is estimated at each gridpoint location as the depth at which the ocean temperature is 1° cooler than the surface temperature. Temperature throughout the model mixed layer [$\tilde{T}(x, y, z, t)$] is then corrected to be consistent with observed surface temperature.

$$\tilde{T}(x, y, z, t) = \begin{cases} \alpha T(x, y, z, t) + (1 - \alpha)\mathrm{SST}(x, y, t), \\ \qquad T(x, y, z, t) \geq T(x, y, 0, t) - 1° \\ T(x, y, z, t), \\ \qquad T(x, y, z, t) < T(x, y, 0, t) - 1° \end{cases} \quad (1)$$

where $\mathrm{SST}(x, y, t)$ is the monthly sea surface temperature analysis of Servain et al. (1987), and $T(x, y, z, t)$ is the model temperature. The size of the parameter α reflects our degree of confidence in the model prediction of mixed-layer temperature. We choose $\alpha = 1/4$, a low value to reflect our belief that the observed surface temperature is more accurate than the model temperature. As more information becomes available on the accuracy of model predictions, this parameter will be adjusted.

c. *Updating with temperature profiles*

In and below the mixed layer a second update is applied to the temperature field using the more accurate, but less frequent, temperature profiles. All binned observations within one month of the analysis time are identified. At each of the 20 model vertical levels between the surface and 484 m, the difference between the temperature observations at that level and SST-corrected first-guess temperatures are computed. These differences we refer to as the temperature residuals $T'(x_n, y_n, z_0, t_n)$. The N temperature residuals for profiles at position (x_n, y_n) and time t_n are defined as

$$T'(x_n, y_n, z_0, t_n) = T^{\mathrm{obs}}(x_n, y_n, z_0, t_n) - \tilde{T}(x_n, y_n, z_0, t), \quad n = 1, 2, 3, \cdots N. \quad (2)$$

An important aspect of four-dimensional data assimilation is that it permits easy quality control of the observations. Some subjective quality control was done on the raw observations. For additional quality control we require that the magnitude of the residuals be within four standard deviations of their mean for each level. Manual checks of the data eliminated by this procedure (some 5% of the total dataset) indicate the criterion is effective in eliminating bad data. Comparing residuals to their neighbors (buddy checking) eliminates only a few data points because of the sparsity of the data, and so buddy checking is not used in the experiments described here.

To map the temperature residuals onto the model grid at each model level we need to determine the influence scale of each observation on the surrounding map gridpoints. These are given by the temporal and spatial lagged correlations of the temperature residuals. To simplify calculation of the correlations we assume that they are homogeneous in space and time. We then calculate the correlation functions from the residuals for analysis A2, the first of the data assimilation experiments, using the following procedure.

To compute the temporal correlation, the temperature residuals are formed into all possible pairs whose locations are separated by 50 km or less, regardless of their location throughout the basin (20°S–20°N). These pairs are grouped into five-day bins according to their time of measurement. Typically each bin contains 200 measurement pairs. The correlation of temperature residuals is then computed within each bin. At 106 m the temperature correlation decreases with increasing time lag with an approximately 40-day exponential timescale (Fig. 3a).

The space-lagged correlations have been computed from the temperature residual pairs whose time differences are less than 10 days. At 106 m the zonal scale is considerably larger (340 km) than the meridional scale (180 km, Fig. 3b). The temperature residuals remain somewhat correlated at zonal lags greater than 600 km. As the depth increases, the spatial lags decrease, although the zonal scale still exceeds the meridional scale (Fig. 3c). For simplicity, in these analyses we neglect the vertical change in the horizontal correlation scale, choosing the correlation at 106 m to represent the correlation throughout the upper ocean. Thus we represent the spatial correlation at all depths by an analytic form which ensures that the variance spectrum of the correlation is positive definite

$$C(\Delta x, \Delta y, \Delta t) = \left(1 + \Delta R + \frac{\Delta R^2}{3}\right) e^{-[\Delta R + (|\Delta t|/40)]}$$

$$\Delta R = \left[\left(\frac{2\Delta x}{340}\right)^2 + \left(\frac{2\Delta y}{180}\right)^2\right]^{1/2}. \quad (3)$$

The actual mapping of the temperature residuals onto the model grid is carried out using (3) in an optimal-interpolation objective analysis procedure which provides the optimal linear mapping that minimizes the mean square temperature error (Gandin 1963). The temperature observations are assumed to contain noise which is 20% of the residual variance. This noise is mainly due to physical processes such as internal waves, which have smaller spatial or temporal scales than we can resolve, rather than error due to the measurements themselves. The objective maps are only weakly dependent on this assumption. For the sake of computational efficiency the analysis is carried out in a series

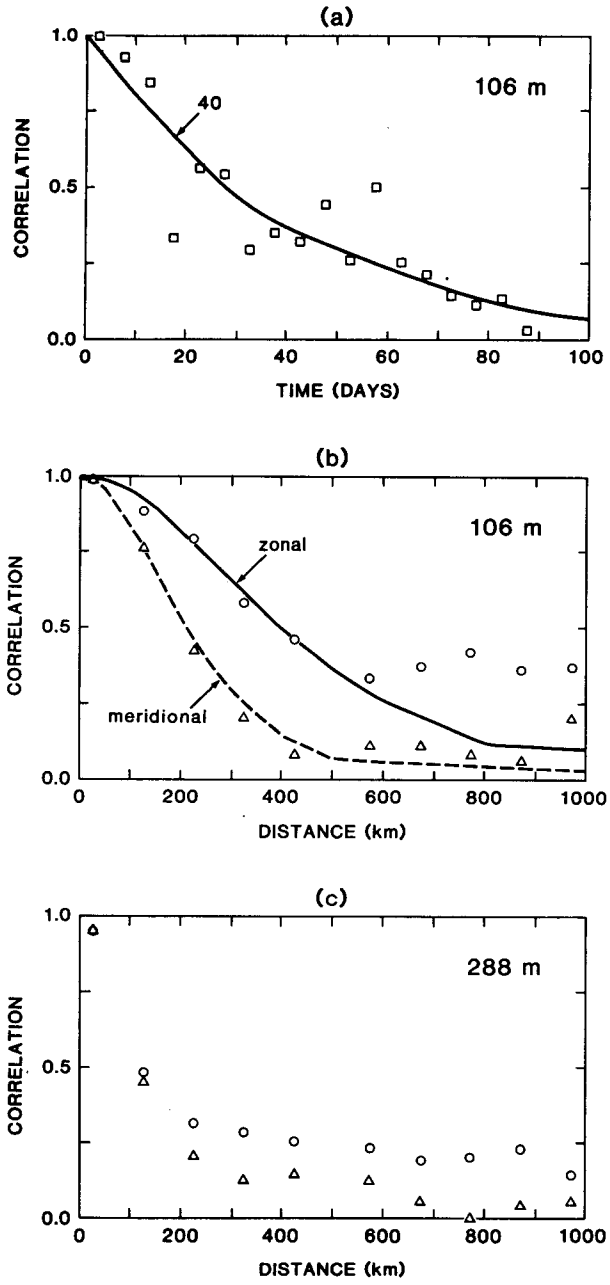

FIG. 3. Correlation of binned temperature residuals and analytical correlation function. (a) Temporal correlation at 106 m depth. (b) Spatial correlation in the zonal (circles) and meridional (triangles) directions at 106 m. (c) Spatial correlation at 288 m.

of patches containing 25 model gridpoints with each patch analysis using the 100 temperature residuals which are most highly correlated with those gridpoints. A detailed description of the procedure is given in Carton and Hackert (1989).

After mapping, the gridded residuals at each level are added to the first-guess temperature field to create the updated field. Because the analysis is carried out level by level, the updating may cause temperature inversions. These inversions generally occur at isolated gridpoints, and are most common at thermocline depths, in regions where the thermocline has large slopes. Inversions are eliminated after several model time steps by convective mixing.

Because little salinity information is available for the tropical Atlantic, the analysis of the salinity field is given by climatological seasonal salinity (which is also used for model initialization). No attempt is made to use model simulated salinity because it has been found that mixing induced by the updating procedure causes the model-simulated salinity fields to become unreasonably uniform. Our current inability to use information about temperature anomalies to update the salinity means that the salinity flux in the model will be incorrect. This may contribute to errors in other dynamical quantities such as mixed-layer depth. The velocity analysis fields are either assumed to be the same as the first-guess fields (A3), or zero (A4).

4. Analyses

A straightforward way to obtain complete fields of temperature, salinity, and velocity is to carry out a numerical simulation of the circulation forced by surface winds and heating. Assimilation of oceanic observations using the procedure outlined above offers one way to improve the analysis. Another analysis approach is based on the observation that monthly variations of density in the tropical Atlantic are dominated by the seasonal cycle. For this reason we also try using seasonal climatology to provide a first guess of the temperature variations. Based on these ideas four analyses of temperature and three of circulation have been created for the 24 month period beginning January 1983. These analyses are described here and summarized in Table 1.

a. Analysis A1: Wind only

This is a simulation of the monthly circulation during 1983–84 without any temperature or salinity updating, carried out by investigators at the Geophysical

TABLE 1. Summary of data assimilation analyses. All analyses begin January 15, 1983 except *A*1 which begins a year earlier. Updating observations consist of surface temperature (SST), temperature profiles (T), and three-dimensional climatological temperature (T_c) and salinity (S_c).

Analysis	Source of first guess	Updating data	Duration (months)
*A*1	model	—	36
*A*2*	T_c, S_c	SST, T	24
*A*3	model	SST, T, S_c	24
*A*4	model	SST, T, S_c, $\vec{V} = 0$	24

* This analysis was repeated with an isotropic correlation function.

Fluid Dynamics Laboratory. Initial conditions are the January temperature and salinity fields produced by running the model with seasonal climatological forcing. The simulation has been carried out for three years beginning January 1982. In this study we will only consider the last two years of the simulation.

b. Analysis A2: Climatology first guess

In this analysis no model integration takes place. The first-guess fields are given by Levitus (1982) monthly climatological temperature. The temperature residuals are the differences between the observations and climatology, except in the mixed layer where they are mainly the differences between the temperature profile observations and the Servain SST dataset. Temperature fields are updated as outlined above. This analysis does not produce velocity fields.

This method of reconstructing the temperature structure is extremely computationally efficient and so qualifies as a "poor man's data assimilation." As an example of the kind of experiments which can be conducted, we have repeated analysis A2 using a spatially isotropic correlation function instead of the usual anisotropic correlation function. The effect of this change on the analysis was minimal. A second strength of this method is that the systematic temperature error is zero if averaged over enough years. The weakness of the method is that anomalous conditions, such as occurred in the first half of 1984, are not predicted in the first guess field. In order to predict these we turn to the ocean model.

c. Analyses A3 and A4: Data assimilation analyses

The first-guess fields of temperature are provided by a month-long numerical simulation. The temperature updating is carried out using the optimal interpolation procedure. The salinity first guess is provided by climatology. The first-guess fields during January, 1983, when the analysis begins, are the same as for analysis A2, that is, climatological salinity and temperature.

Velocity observations are far too limited to update the first-guess field. This means that large errors exist in the velocity analysis field and that the velocity analysis is not in geostrophic balance with the temperature analysis. We test the sensitivity of using unbalanced initial conditions by making an extreme assumption in A4, setting the velocity field to zero when initializing the model. The A4 analysis velocity is the velocity provided by the numerical model after a month's integration, as for A3. As we shall see, this has little impact on the analysis.

5. Gross temperature accuracy

Several datasets are available for us to verify the accuracy of the analyses. The first is a subset of the set of temperature residuals generated in the course of the data assimilation cycle. For verification we choose only temperature residuals $[T'(x_n, y_n, z_0, t_n)]$ from the month in which the update takes place so that $|t_n - t| < 15$ days. If the residuals were very small this would be evidence that the first-guess temperature fields are highly accurate over broad areas. If the residuals were very large this would be evidence that the analysis is inaccurate, except where observations are available. We first estimate the systematic (time mean) error of each analysis by time averaging the residuals T' in $1° \times 1°$ bins at each vertical level throughout the two-year period. We then objectively map the averaged residuals $\overline{T'}(x_n, y_n, z_0)$ onto the model grid. The size of the mean residual reflects the error in the first-guess field. The accuracy with which it is estimated deteriorates north of 10°N due to the limited number of residuals.

The largest systematic errors show up in A1 (Fig. 4a). The simulated thermocline is too high by 20 m or so all along the equator except in the far west. This causes a cool anomaly (model cooler than observations) at thermocline depths, of up to 2°C—near-surface in the east but deepening to 120 m in the west. However, the surface temperatures are too warm in the east by one degree. When combined with the upward shift of the thermocline, this means that the model has much too strong thermal stratification in the east. The water in the couple of hundred meters below the thermocline is too warm by up to 2°C. Similar mean errors appear in comparison with mooring observations in section 7.

At 30°W the systematic error for A1 is largest poleward of ±5° latitude, with the largest errors in the southern hemisphere (Fig. 5a). These large errors are cool anomalies associated with anomalous lifting of the thermocline. North of the equator the simulation underestimates the depth of the trough in the thermocline between the equator and 5°N associated with the North Equatorial Countercurrent (NECC) shown also in Fig. 6. Between 10° and 20°N the error again increases, this time as a result of limited, unrepresentative data coverage. Surface temperatures are too warm throughout the tropics.

The systematic error for the other analyses is much lower. The only coherent feature in the systematic error of A2 is that the thermocline is still too shallow in the central equatorial basin (Fig. 4b). At 30°W the errors are much reduced, although warm anomalies indicate that the thermocline troughs are also too weak in the temperature climatology (Fig. 5b). The systematic temperature errors for A3 show the thermocline is still too shallow in the east with 2°C anomalies, similar to A1. But in the central and western basin the thermocline is slightly too deep, with much reduced anomalies compared to A1 (Fig. 4c). At the western edge of the transect the model, hence A1 and A3, is consistently too warm due to local effects near the Brazil coast. At 30°W the thermocline troughs are well represented in A3 (Fig. 5c). A similar improvement in the depth of

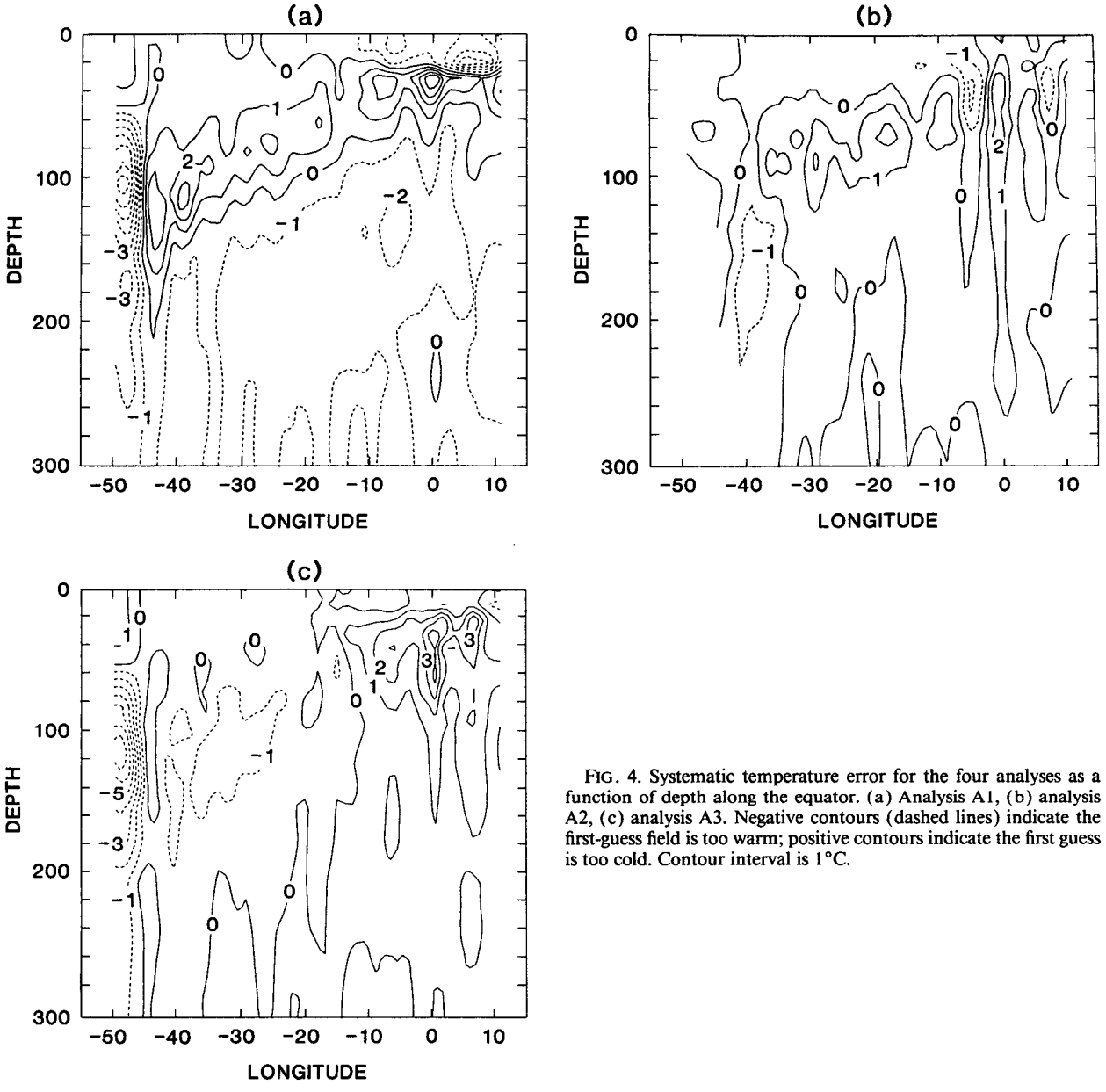

FIG. 4. Systematic temperature error for the four analyses as a function of depth along the equator. (a) Analysis A1, (b) analysis A2, (c) analysis A3. Negative contours (dashed lines) indicate the first-guess field is too warm; positive contours indicate the first guess is too cold. Contour interval is 1°C.

the thermocline, although of different sign near the equator, is shown by Leetmaa and Ji (1989).

Variability of temperature residuals

The large systematic error of analysis A1 is evidence that our numerical model is less accurate than climatologies in estimating the mean stratification. The real usefulness of models such as this comes in their ability to predict variations in the state of the ocean due to variations in surface forcing. To estimate the accuracy of the first guess fields of each analysis in predicting these variations we examine a mean-square average of the residuals for the month (t) in which the updating is done, subtracting the systematic error.

$$E(t) = \frac{1}{N(t)} \sum_{n=1}^{N(t)} [T'(x_n, y_n, z_0, t_n) - \overline{T'}(x_n, y_n, z_0)]^2 \quad (4)$$

where $N(t)$ is the number of observations in each month. The variance is in degrees squared so the variability in degrees is the square root of this quantity.

Analysis A1 has errors in temperature variability which exceed 2°C in the thermocline throughout much of the two-year period (Fig. 6a). The large errors in the summer and fall of 1983 are from data between

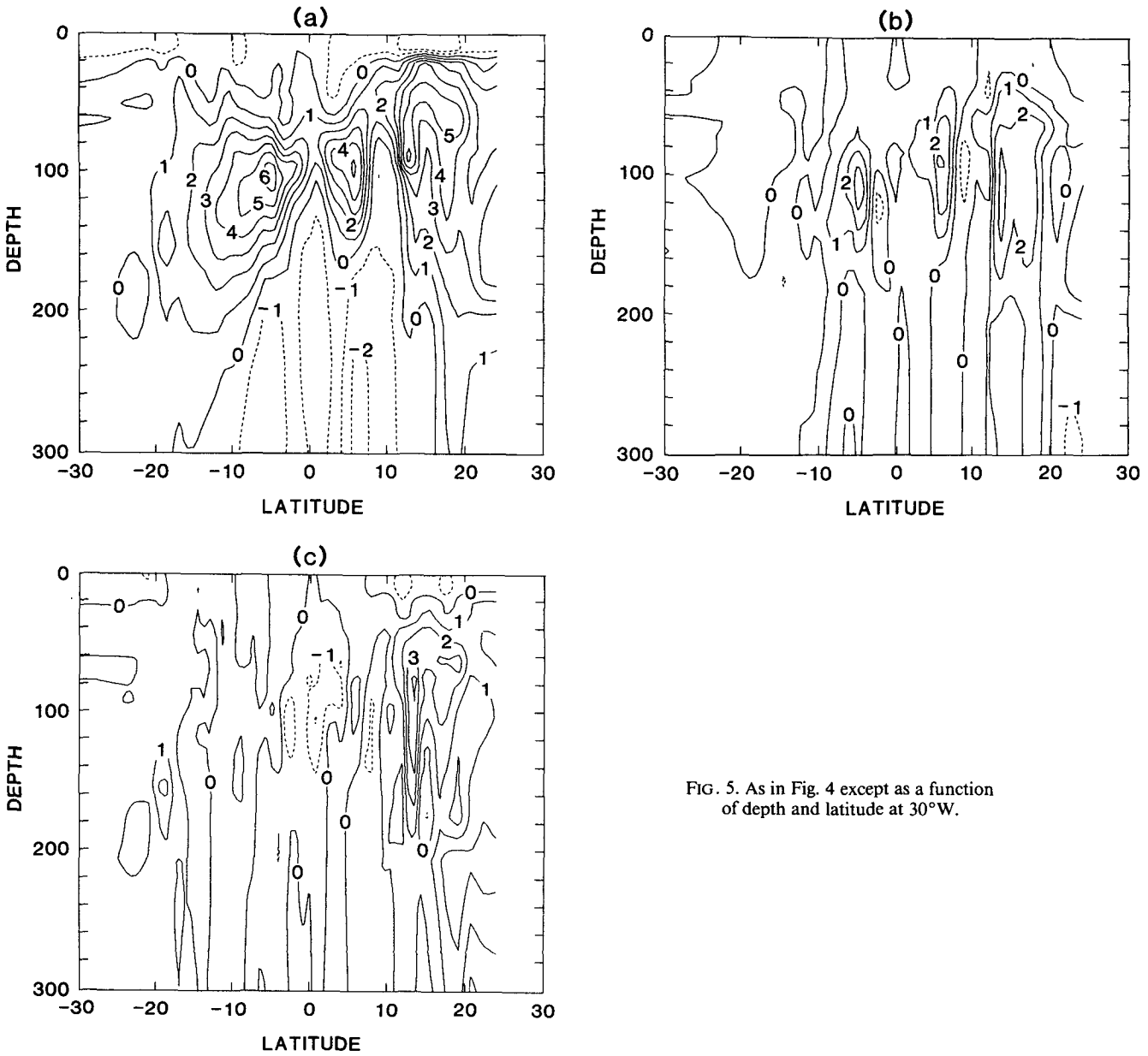

FIG. 5. As in Fig. 4 except as a function of depth and latitude at 30°W.

the equator and 10°N. They are partly due to underestimation of the depth of the NECC trough and misrepresentation of the disappearance of the trough in early spring (also discussed in section 7). The increase in error in March and September in all four analyses results from the intensive data coverage in the high variability region off the coast of Brazil (see Fig. 2) which is not represented correctly by either the climatology or the model.

The error variability for A2 is reduced by a factor of two over A1 (Fig. 6b). It is interesting to see that the error increases in the first half of 1984 because of the inability of climatology to represent the unusually deep thermocline displacement associated with the 1984 warm anomaly in the Gulf of Guinea (Fig. 6c). The error increases late in 1984 because of limited, unrepresentative data coverage in all analyses. Derber and Rosati (1989) find somewhat lower errors in the tropics (between 3 and 4 $(°C)^2$, their Fig. 6). However, their statistics were computed by subtracting the observations from the analysis, rather than the first-guess estimate, and so are not directly comparable.

6. Thermal gradients

Much of the seasonal change in heat storage occurs by a meridional transport of water into the NECC trough between the equator and 10°N, and by a zonal

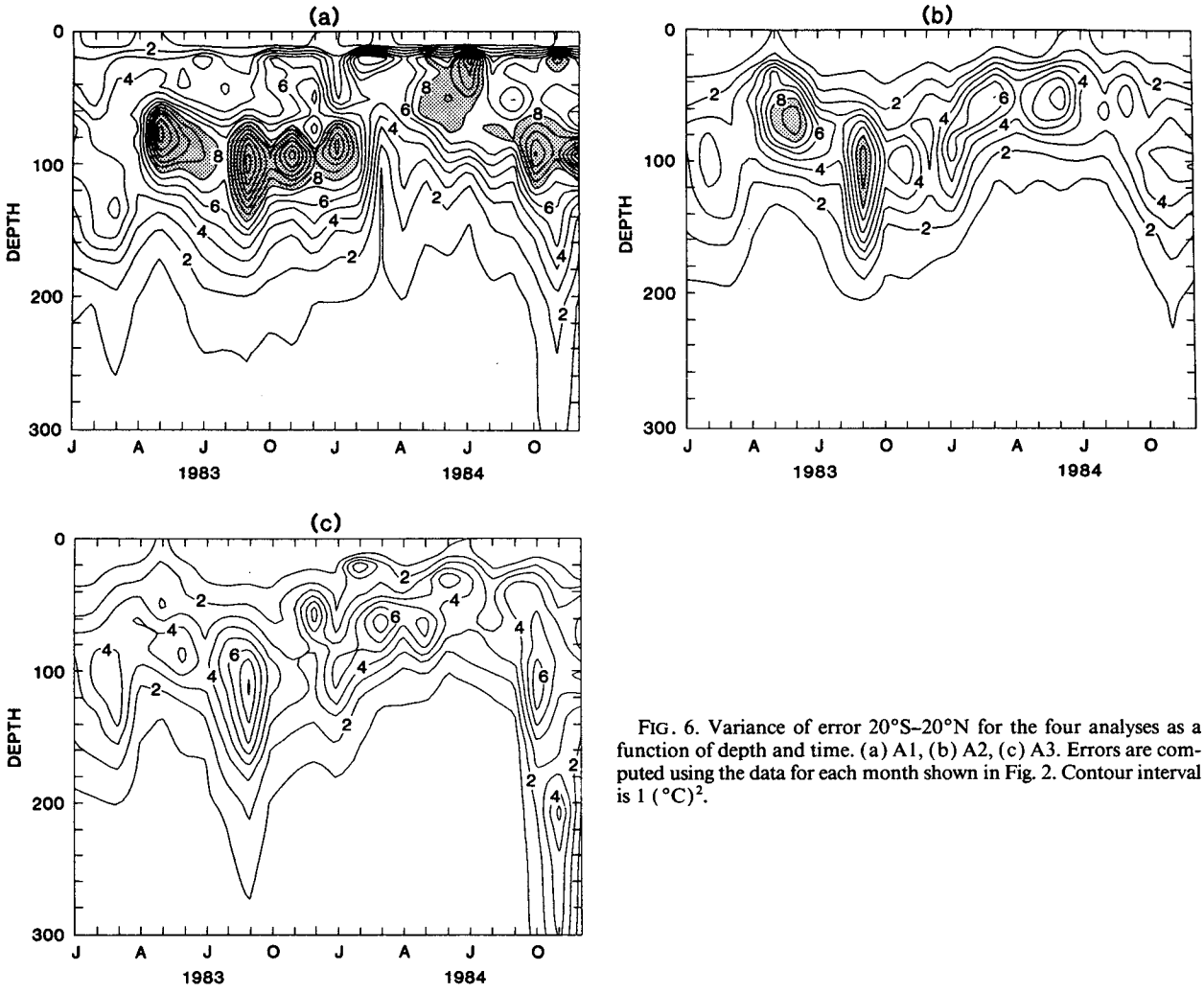

FIG. 6. Variance of error 20°S–20°N for the four analyses as a function of depth and time. (a) A1, (b) A2, (c) A3. Errors are computed using the data for each month shown in Fig. 2. Contour interval is 1 $(°C)^2$.

shift of warm water along the equator. This makes proper representation of the phase and amplitude of these changes crucial. Beginning in February 1983 a series of inverted echo sounders were deployed at ten locations in the tropical Atlantic. The instruments record acoustic travel time which can be linearly related to 0/500 m average temperature, which in turn is proportional to heat storage. We begin by focusing our attention on meridional changes.

a. Meridional gradient

Using two sets of three inverted echo sounder moorings to estimate the temperature gradient, Katz (1987) computed differences between the average temperature at the equator, 3°N and 9°N, at longitudes of 38°W, and 28°W. Between latitudes 3° and 9°N the temperature gradient has a strong seasonal cycle reaching its most negative in the boreal summer and fall (observations are shown in bold in Figs. 7 and 8). During fall the temperature difference resulting from this gradient exceeds 3°C at 38°W and 1.5°C at 28°W, as warm water piles up near the equator and the NECC intensifies (Figs. 7a, 8a). Half a year later as the equatorial trade winds weaken, the temperature difference at 38°W actually changes sign. At 28°W the temperature difference weakens, but not as abruptly, and the gradient does not actually change sign. Between the equator and 3°N the phase of the seasonal cycle is reversed. Here the gradient is most positive in summer, with annual changes of 2°C at 38°W, but with low amplitude at 28°W (Figs. 7b, 8b).

The phase agreement between these observations and the numerical simulation is good; the average correlation for the five gradient time series is 0.74. But the agreement of amplitude is poor. At 38°W for example, the amplitude of the seasonal variation for A1 is one-third of the observed. At 28°W the agreement with A1 is better, but the amplitude is still too low in the band 3°–9°N. Root-mean-square differences between the observations and analyses are summarized in Table 2.

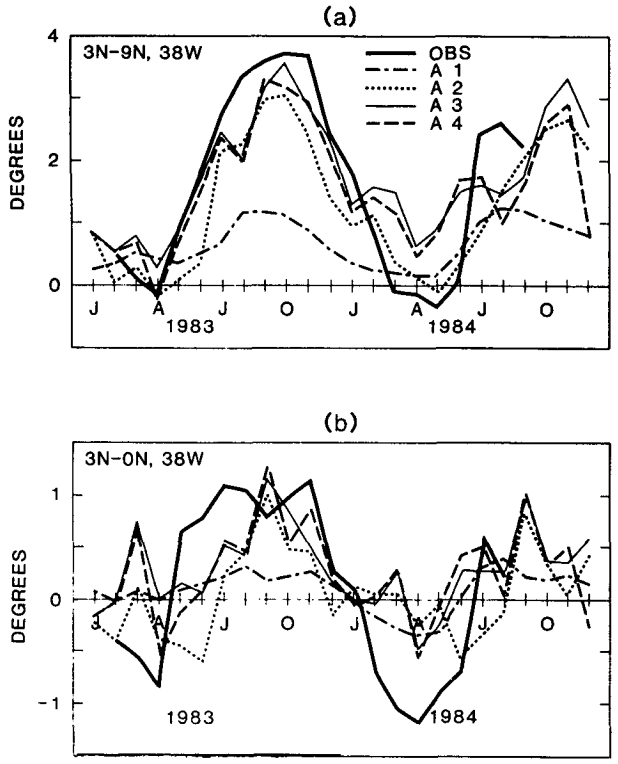

FIG. 7. Average 0/500 m meridional temperature difference at 38°W. (a) Between 3° and 9°N and (b) 3°N and 0°. Bold curves are monthly averaged observations (redrawn from Katz 1987).

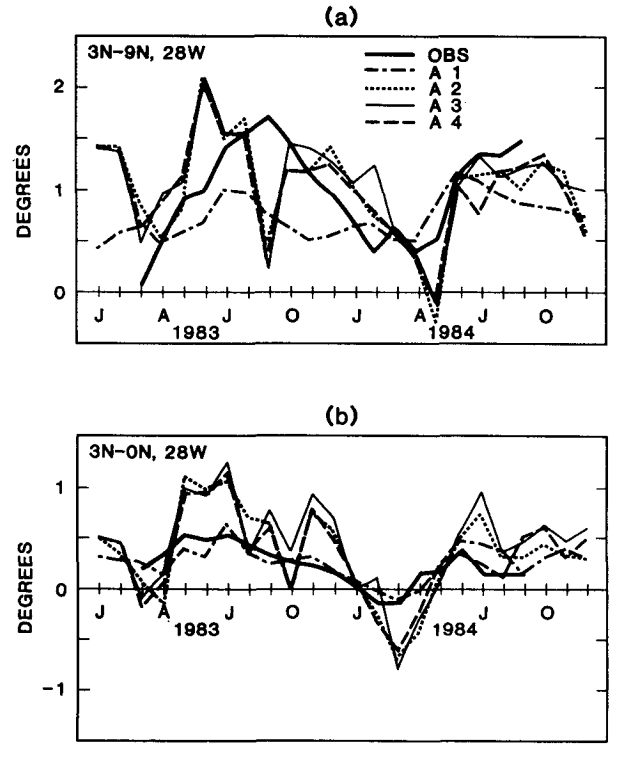

FIG. 8. As in Fig. 7 but at 28°W.

TABLE 2. Root-mean-square differences between monthly averaged observed 0/500 m temperature differences and those produced by the four analyses for three pairs of moorings (ΔT_{rms}). The root-mean-square of the observed temperature differences (T_{rms}) are included for comparison.

Station pairs	T_{rms} (°C)	ΔT_{rms} A1	A2	A3	A4
$\bar{T}$(3°N, 38°W) − $\bar{T}$(9°N, 38°W)	1.4	1.5	0.8	0.8	0.8
$\bar{T}$(3°N, 38°W) − $\bar{T}$(0°N, 38°W)	0.8	0.6	0.7	0.7	0.7
$\bar{T}$(3°N, 28°W) − $\bar{T}$(9°N, 28°W)	0.5	0.5	0.5	0.5	0.5
$\bar{T}$(3°N, 28°W) − $\bar{T}$(0°N, 28°W)	0.2	0.1	0.4	0.4	0.3
$\bar{T}$(0°N, 10°W) − $\bar{T}$(0°N, 34°W)	0.5	0.8	0.7	0.6	0.7

When the analyses are updated with hydrographic observations the amplitude of the seasonal variation increases substantially giving closer agreement, but still with weaker gradients, than observed. This is most evident for the mooring pair (3°–9°N, 38°W), which has the strongest seasonal variation. At 28°W the results from the three analyses using data assimilation are similar in accuracy to those obtained from A1. The higher errors of A2–A4 at 3°N–0°, 28°W result from a less attractive feature of the updating, which is that it introduces strong month-to-month noise (discussed in section 7).

Another characteristic of the analyses using data assimilation is that they are more similar to each other than to the observation time series. Frequently the analyses for a given month all differ from the inverted echo sounder observations by the same substantial amount (e.g., in September at 3°–9°N, 28°W). The likely explanation for this is that individual hydrographic observations used to update the analyses can have different values than nearby estimates from the inverted echo sounder data used to verify the analyses.

b. Zonal gradient

Like the meridional temperature gradient, the zonal gradient along the equator undergoes a strong seasonal

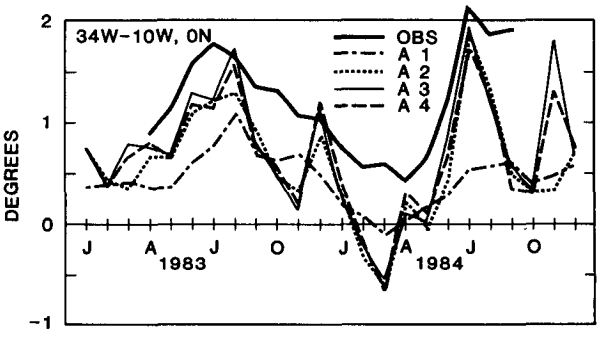

FIG. 9. Average 0/500 m zonal temperature difference along the equator between 34° and 10°W. Bold curve is monthly averaged observations (redrawn from Katz 1987).

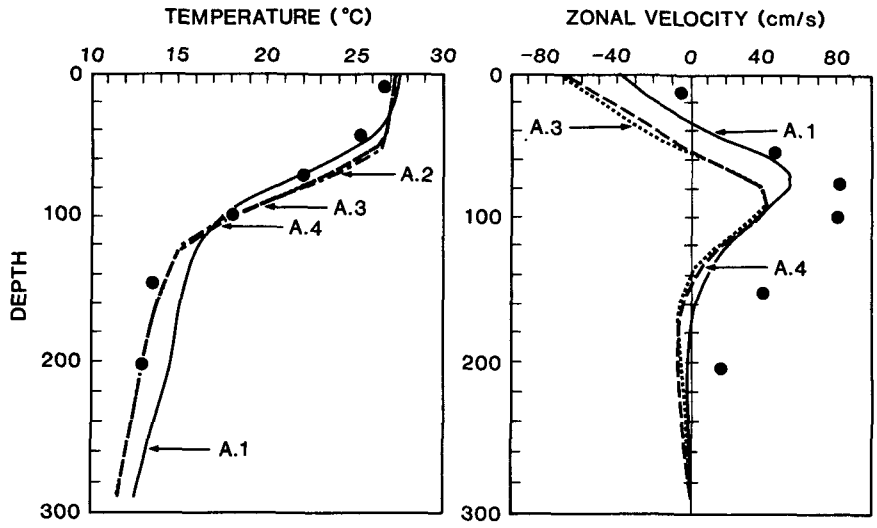

FIG. 10. Temperature and zonal velocity with depth, averaged from March 1983 through September 1984 at 0°N, 28°W. Mean observations are indicated by dots.

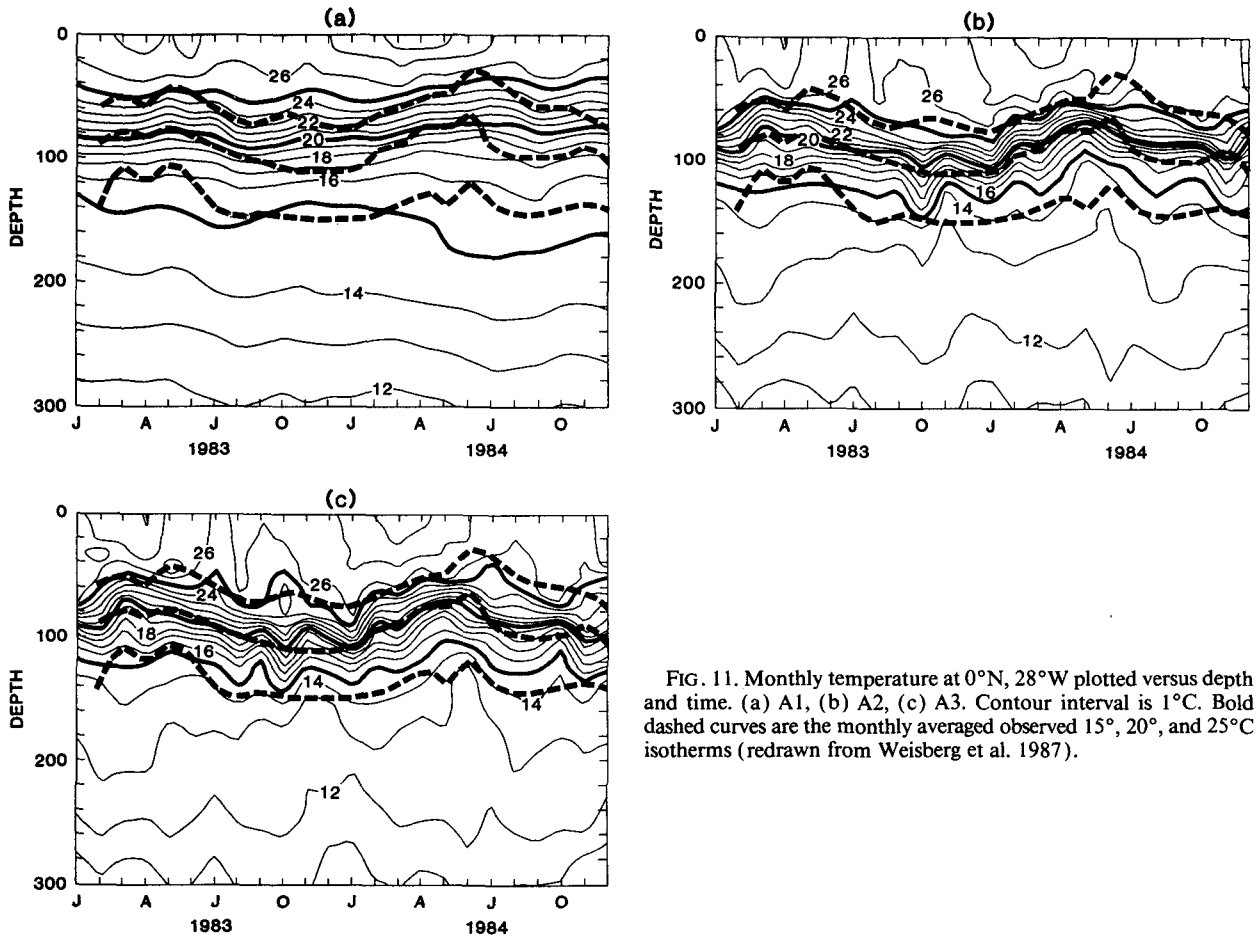

FIG. 11. Monthly temperature at 0°N, 28°W plotted versus depth and time. (a) A1, (b) A2, (c) A3. Contour interval is 1°C. Bold dashed curves are the monthly averaged observed 15°, 20°, and 25°C isotherms (redrawn from Weisberg et al. 1987).

cycle (bold curve in Fig. 9). The temperature difference between 10°–34°W varies from a minimum of 0.4°C in late boreal winter and spring to greater than 1.5°C in summer with the increase occurring more abruptly in 1984 than in 1983.

As in the case of the meridional gradient, the zonal gradient amplitude of the annual cycle for A1 is too weak, in comparison with observations, although the phase is reasonable. The disagreement increases in 1984 when the observed zonal gradient strengthens dramatically. The data assimilation analyses compare better with the observations, and in particular, show the rapid increase in gradient observed in the spring of 1984. The month-to-month variability of the analyses, however, is again too large.

7. Midbasin temperature and velocity mooring comparisons

Two direct comparisons with observations of temperature and velocity are available at 28°W, from moorings in the undercurrent (0°N) and at the latitude of the climatological NECC (6°N). The equatorial mooring was maintained at six depths between 10 and 200 m throughout the experiment beginning in February 1983 (Weisberg et al. 1987), while the mooring at 6°N was maintained from Februrary 1983 until October 1984 (Levy and Richardson 1984; Levy and Richardson 1985).

a. 0°N

At this midbasin location mild vertical shifts of the thermocline result from both local Ekman divergence and remote forcing. The two-year average depth of the observed thermocline, which corresponds to the depth of the core of the undercurrent, lies between 50 and 100 m (time averaged in Fig. 10 and plotted with time in Figs. 11 and 12). Without assimilation, A1 produces a thermocline which is too diffuse and elevated by 20 m. With assimilation (A3) the vertical position of the thermocline is more accurate, however the mean speed of the westward surface South Equatorial Current is too strong (>40 cm s^{-1}) and the undercurrent is too weak (<40 cm s^{-1}).

The weak seasonal changes in the depth of the undercurrent core are linked to seasonal changes in thermocline depth, which is evident by comparing Figs. 11 and 12. These seasonal changes are stronger in A2 and A3 in the thermal field, and A4 in current than A1. The spring rising of the thermocline in A1 occurs mainly in isotherms between 20° and 25°C rather than throughout the thermocline as observed (compare Fig. 11a with Weisberg et al. 1987, Fig. 5). The time series also shows evidence of long-term warming of the subthermocline water, as the 15°C isotherm appears to have left the thermocline by 1984. In contrast, A3 shows seasonal changes of its thermocline which are

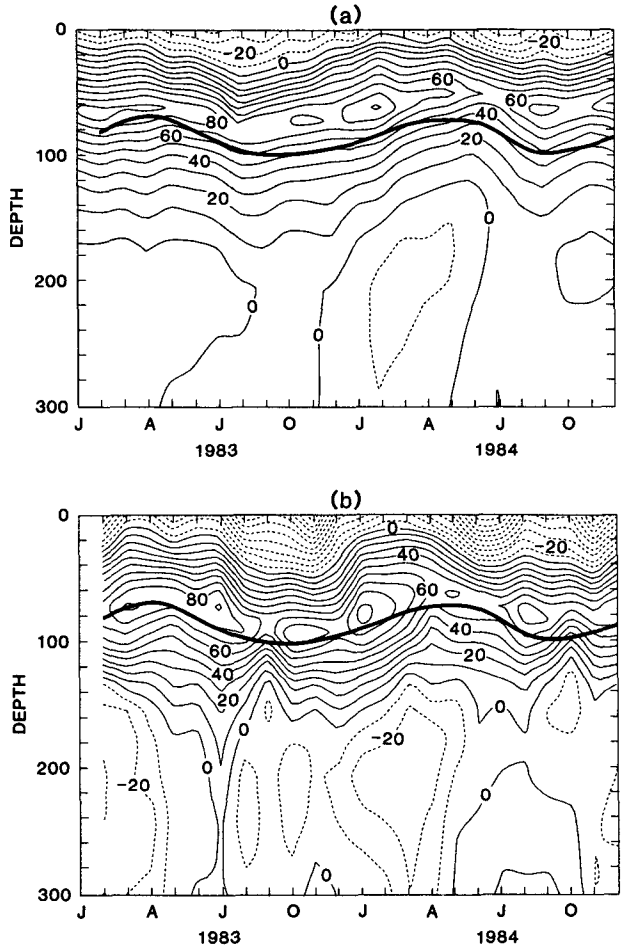

FIG. 12. Monthly zonal velocity at 0°N, 28°W plotted versus depth and time. (a) A1, (c) A3. Contour interval is 10 cm s^{-1}. Negative (dashed) contours denote westward currents. Bold curve is the depth of the monthly averaged observed undercurrent core (redrawn from Weisberg et al. 1987).

visually similar to observations, shallowing in spring of both years—enough so that the 25°C isotherm reaches 50 m depth.

One issue raised by the updating procedure is the intensity of noise introduced by the updating itself. Since the ocean is forced by monthly winds, much of the fluctuations in zonal velocity in the analyses for example is due to the updating procedure. At 75 m depth the monthly zonal velocity has an rms variability of 13 cm s^{-1}, around a mean zonal current of 65 cm s^{-1}. The rms variability computed from three-day sampled data increases to 17 cm s^{-1} because of the high frequency noise induced by the updating.

The zonal dependence of the undercurrent strength and elevation is shown for August, 1984 in Fig. 13, along with instantaneous observations of zonal current from Henin et al. (1986) and Hisard and Henin (1987). The observed undercurrent slopes up to the east with the high speed core penetrating all the way

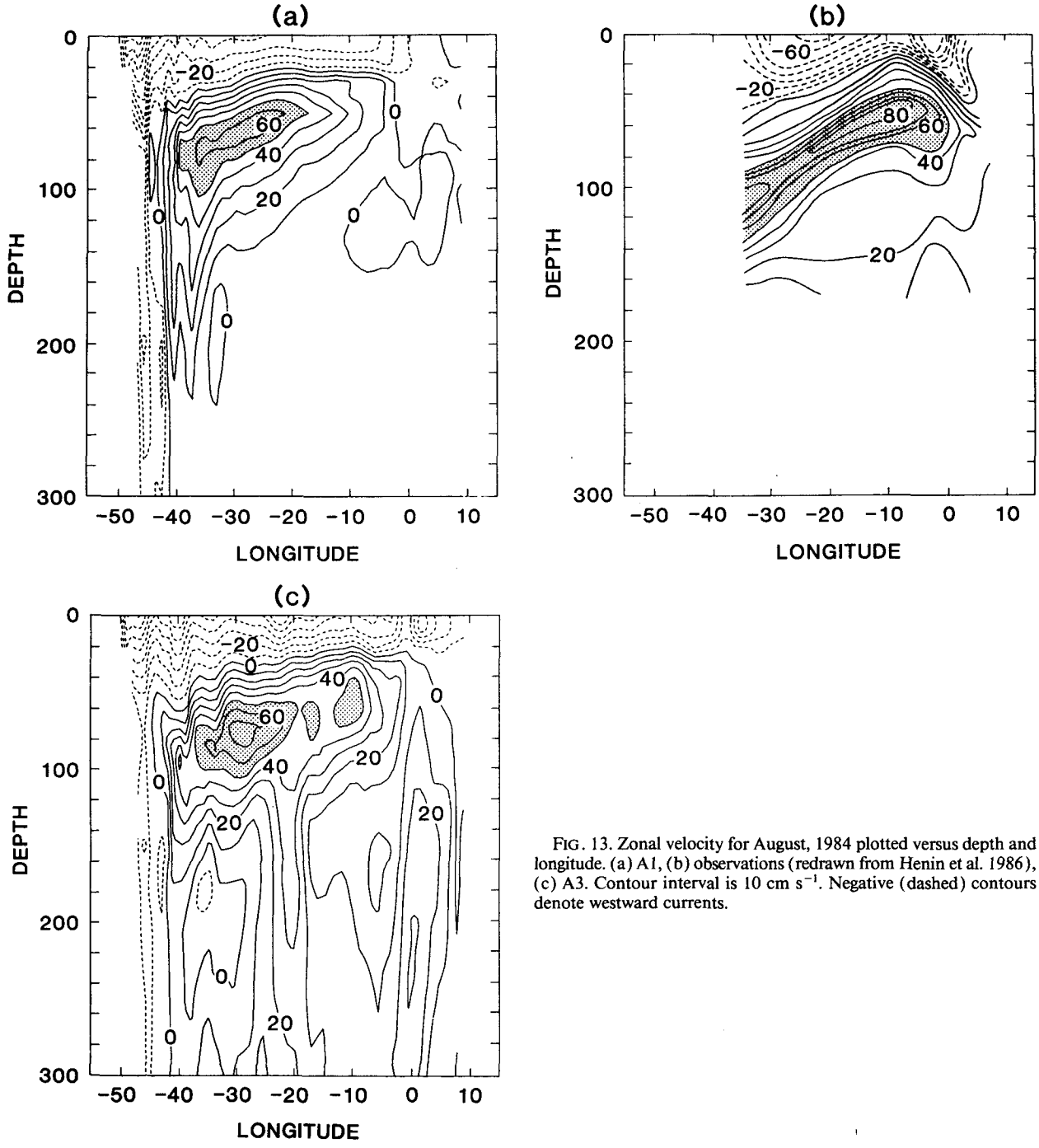

FIG. 13. Zonal velocity for August, 1984 plotted versus depth and longitude. (a) A1, (b) observations (redrawn from Henin et al. 1986), (c) A3. Contour interval is 10 cm s^{-1}. Negative (dashed) contours denote westward currents.

to 0°E, and weaker eastward flow to at least 4°E. The analyses have weaker maximum speeds than observed (Figs. 13a,c). However, only A3 and A4 (not shown) penetrate realistically eastward into the Gulf of Guinea.

b. 6°N

At this site temperature records were maintained throughout the period at 20, 50, 75, and 150 m depths, while complete velocity measurements are only available at 20 and 150 m. A description of the velocity measurements is provided in Richardson and Reverdin (1987).

Because conditions at this location vary considerably depending on whether the seasonal NECC is present, we compare vertical profiles of temperature and zonal current averaged July through December 1983 and July through September 1984, months when both the cur-

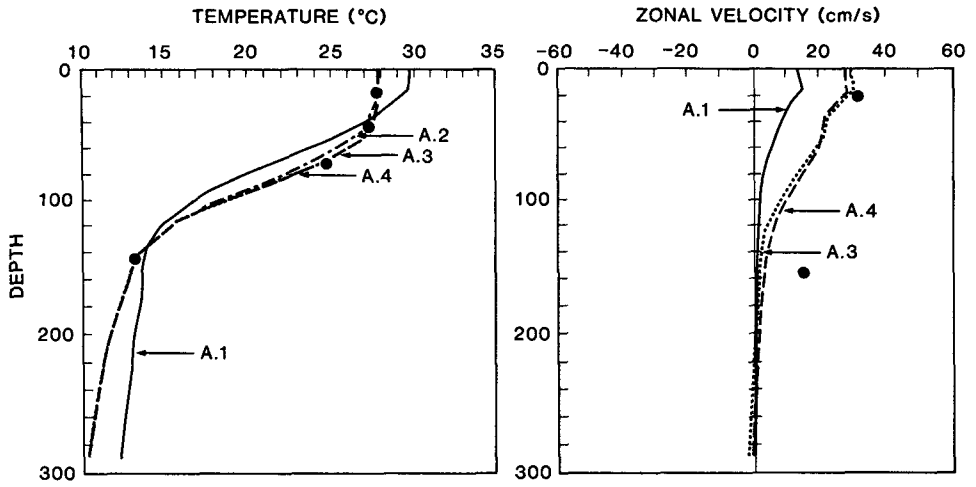

FIG. 14. Temperature and zonal velocity with depth at 6°N, 28°W, averaged from July through December 1983 and July through September, 1984 (months when the NECC is strong). Mean observations are indicated by dots.

rent and the mooring observations are available. These mean profiles are shown in Fig. 14 and listed in Table 3. The position and sharpness of the observed thermocline is within 1°C of the thermocline of A2, with even better agreement (= <0.5°C) with A3–A4. As indicated before, A1 is too warm nearsurface and below the thermocline. The thermocline itself is displaced vertically (Fig. 14a) so that the temperatures at 50 and 75 m are more than 2°C too cold.

The mean zonal current is 31 cm s^{-1}, which is reasonably simulated by A3–A4, but as suggested by the temperature comparisons of sections 5 and 6, the A1 current is much too weak (Fig. 14b). The observed current extends below the thermocline (15 cm s^{-1} at

TABLE 3. Mean and root-mean-square deviations of monthly temperature and zonal velocity between mooring observations (T_{obs} and U_{obs}) at 6°N, 28°W and those produced by the four analyses (T_{anal} and U_{anal}).

Analysis	Depth (m)	$\bar{T}$*	$\overline{\Delta T}$† (°C)	ΔT_{rms}† (°C)	$\bar{U}$*	$\overline{\Delta U}$†	ΔU_{rms}† (cm s^{-1})
Mooring	20	27.7		0.7	31.		17.
observation	50	27.2		0.7			
	75	24.5		2.1			
	150	13.8		1.1	15.		11.
A1	20	29.1	−1.8	0.6	13.	12.	14.
	50	25.3	2.4	1.2			
	75	20.8	2.9	1.7			
	150	13.5	−0.4	1.1	1.	6.	12.
A2	20	27.8	−0.3	0.5			
	50	26.4	0.8	0.8			
	75	23.1	0.9	2.0			
	150	13.0	0.2	1.0			
A3	20	27.8	−0.3	0.5	28.	1.	14.
	50	26.7	0.5	0.7			
	75	23.1	0.5	1.8			
	150	12.8	0.4	0.9	3.	5.	12.
A4	20	27.8	−0.3	0.5	27.	5.	14.
	50	26.9	0.5	0.9			
	75	23.4	0.5	1.8			
	150	12.9	0.3	0.9	1.	6.	12.

* Computed during the periods when the North Equatorial Countercurrent is strong (July through December, 1983 and July through September, 1984).

† $\Delta T \equiv T_{anal} - T_{obs}$, $\Delta U \equiv U_{anal} - U_{obs}$. For the entries under Mooring Observations the square root of the observation variance is given. These statistics have been computed using the full 19-month time series.

150 m, Table 3) unlike any of the analyses. The reason for this striking difference needs to be explored.

The temporal variation of zonal velocity at 20 m is shown in Fig. 15. Along with more realistically strong velocities, the analyses A3 and A4 have a more realistically strong seasonal cycle, although some errors are evident. For example they show a delay in the initiation of the NECC in 1984 by one month compared to the observations. Despite this, the rms differences between the analyses and 20 m zonal velocity, are the same, 14 cm s^{-1} (Table 3).

8. Discussion

Assimilation of oceanographic data into a numerical model offers a way of improving the quality of the model-derived fields of temperature and velocity. Here we apply the technique of four-dimensional data assimilation to the tropical Atlantic to construct a monthly analysis of the circulation and temperature changes for the two-year period 1983–84. In this implementation of the method the first guess of the temperature fields is provided by the model of Philander and Pacanowski (1986). This first guess is updated monthly by objectively analyzing the residual differences between temperature profiles and the first guess. We find that the method can be applied in a straightforward way to provide reasonable analyses.

To determine the sensitivity of the results to the observation dataset we compare the data assimilation analysis to a numerical simulation with no updating. To determine the sensitivity of the analysis to the first-guess fields and initial conditions, we construct two more alternative analyses, one using climatological temperature instead of the model to provide the first guess and the other using a zero velocity field initial condition for reinitialization.

Comparisons within in situ data show that the numerical simulation has substantial time-averaged biases, including a thermocline which is too high, and excessive stratification in the Gulf of Guinea. The systematic misplacement of the thermocline causes errors in the month-to-month temperature variability as well.

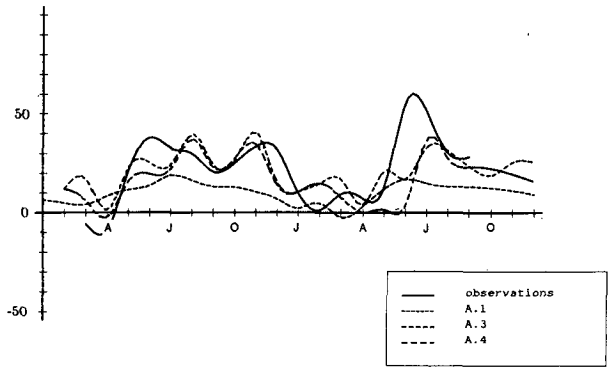

FIG. 15. Monthly zonal velocity at 20 m depth, 6°N, 28°W.

Assimilation of data deepens the trough in the thermocline associated with the North Equatorial Countercurrent. Assimilation also increases the slope of the thermocline along the equator and gives a more realistic representation of interannual changes, such as the anomalous change in zonal thermocline slope in February–July 1984.

Updating the temperature field changes the velocity field as well. The North Equatorial Countercurrent is intensified and the undercurrent extends further eastward, in agreement with observations. Interestingly, similar improvements in the thermal gradients and strengthening of the currents have been found to result from data assimilation in the Pacific Ocean by Hayes et al. (1989).

One issue of concern is the lack of updating information for the velocity field. Comparison of data assimilation with and without velocity initial conditions shows that in the tropical Atlantic the velocity initial condition is unimportant by the time the monthly analysis is made. At 6°N, 28°W the difference in velocity initial condition reduces the strength of the NECC by only 1 cm s^{-1}. In contrast, in the Pacific the results of Philander et al. (1987, their Fig. 6) and Moore (1989) indicate that velocity initial conditions will affect the analysis in the eastern basin for well over a month. The difference is a result of the larger Pacific basin size.

Another way in which the Atlantic differs from the Pacific Ocean is the high degree with which variability is dominated by the annual cycle. This is the reason why data assimilation using a climatological temperature first guess is so successful. Strong justification for using a numerical model in the analysis of temperature will require correcting the surface forcing fields and model-induced errors in the first-guess fields. The wind and surface heating products available from the weather prediction centers have improved substantially since the surface products used in this study were created. Improvements in model parameterizations such as mixing are also underway. With improvements in the forcing fields and enhanced datasets provided by altimetry; for example, the prospect is very bright for creating accurate ocean analyses for use in studies of the dynamical balances and transport characteristics of the seasonal tropical Atlantic Ocean.

Acknowledgments. The authors are grateful to G. Philander and W. Hurlin at GFDL for providing the numerical simulation, and to the SEQUAL/FOCAL investigators for giving us access to the observation data set. J. L. Kinter, III, J. Derber, and E. Katz and two reviewers provided useful comments on an earlier version of this manuscript. We thank J. Merle for allowing us to reproduce Fig. 1. This work has been supported by the National Science Foundation (OCE-86-10422).

Computer resources have been provided by the San Diego Supercomputer Center.

REFERENCES

Carton, J. A., and E. Hackert, 1989: Applications of multivariate statistical objective analysis to the circulation in the tropical Atlantic Ocean. *Dyn. Atmos. Oceans,* **13,** 491–515.

Derber, J., and A. Rosati, 1989: A global data assimilation system. *J. Phys. Oceanogr.,* **19,** 1333–1347.

Gandin, L. S., 1963: *Objective Analysis of Meteorological Fields.* Leningrad Hydrometeorology Press,

Ghil, M., 1989: Meteorological data assimilation for oceanographers. Part I: Description and theoretical framework. *Dyn. Atmos. Oceans,* **13,** 171–218.

Hayes, S., M. J. McPhaden and A. Leetmaa, 1989: Observational verification of a quasi-real-time simulation of the tropical Pacific Ocean. *J. Geophys. Res.,* in press.

Henin, C., P. Hisard and B. Piton, 1986: Hydrographic observations in the Equatorial Atlantic Ocean (July 1982–August 1984), Institut Français de Recherche Scientifique pour le Développment en coopération. ORSTOM, Paris, 191 pp.

Hisard, P., and C. Henin, 1987: Response of the equatorial Atlantic Ocean to the 1983–84 wind from the FOCAL cruise data set. *J. Geophys. Res.,* **92,** 3759–3768.

Katz, E. J., 1987: Seasonal response of the sea surface to the wind in the equatorial Atlantic. *J. Geophys. Res.,* **92,** 1885–1893.

Leetmaa, A., and M. Ji, 1989: Operational hindcasting of the tropical Pacific. *Dyn. Atmos. Oceans,* in press.

Levitus, S., 1982: Climatological Atlas of the world ocean, NOAA Prof. Paper 13, U.S. Department of Commerce, Rockville, MD, 174 pp.

Levy, E., and P. L. Richardson, 1984: Moored Current Meter Data from the Atlantic North Equatorial Countercurrent near 6N 28W (September 1983–March 1984). Woods Hole Oceanographic Institution Tech. Rep. 84–37.

——, and P. L. Richardson, 1985: Moored current meter data from the Atlantic North Equatorial Countercurrent near 6N 28W (March–October 1984). Woods Hole Oceanographic Institution Tech. Rep. 85–7.

Merle, J., 1980: Seasonal heat budget in the equatorial Atlantic Ocean. *J. Phys. Oceanogr.,* **10,** 464–469.

Moore, A. M., 1989: Aspects of geostrophic adjustment during tropical ocean data assimilation. *J. Phys. Oceanogr.,* **19,** 435–461.

——, N. S. Cooper and D. L. T. Anderson, 1987: Initialization and data assimilation in models of the Indian Ocean. *J. Phys. Oceanogr.,* **17,** 1965–1977.

Pacanowski, R. C., and S. G. H. Philander, 1981: Parameterization of vertical mixing in numerical models of tropical oceans. *J. Phys. Oceanogr.,* **11,** 1443–1451.

Philander, S. G. H., 1986: Unusual conditions in the tropical Atlantic Ocean in 1984. *Nature,* **222,** 236–238.

——, and R. C. Pacanowski, 1986: A model of the seasonal cycle of the tropical Atlantic Ocean. *J. Geophys. Res.,* **91,** 14 192–14 206.

——, W. Hurlin and R. C. Pacanowski, 1987: Initial conditions for general circulation models of tropical oceans. *J. Phys. Oceanogr.,* **17,** 147–157.

Richardson, P., and G. Reverdin, 1987: Seasonal cycle of velocity in the Atlantic North Equatorial Countercurrent as measured by surface drifters, current meters, and ships. *J. Geophys. Res.,* **92,** 3691–3708.

Robinson, A. R., J. A. Carton, N. Pinardi and C. N. K. Mooers, 1986: Dynamical forecasting and dynamical interpolation: An experiment in the California Current. *J. Phys. Oceanogr.,* **16,** 1561–1579.

Servain, J., M. Seva, S. Lukas and G. Rougier, 1987: Climatic atlas of the tropical Atlantic wind stress and sea surface temperature, 1980–1984. *Ocean-Air Interactions,* **1,** 109–182.

Teague, W. J., E. J. Molinelli and M. J. Carron, 1987: A new system for management of the "Master Oceanographic Observation Data Set" (MOODS). *Eos,* **68,** 553–559.

Weisberg, R. H., J. H. Hickman, T. Y. Tang and T. J. Weingartner, 1987: Velocity and temperature observations during the Seasonal Response of the Equatorial Atlantic Experiment at 0N, 28W. *J. Geophys. Res.,* **92,** 5061–5075.